Available online at www.sciencedirect.com

SciVerse ScienceDirect

Advances in Space Research 51 (2013) 1842–1856

ADVANCES IN SPACE RESEARCH (a COSPAR publication)

www.elsevier.com/locate/asr

Very intense geomagnetic storms and their relation to interplanetary and solar active phenomena

N.S. Szajko [a,*], G. Cristiani [a,b,1], C.H. Mandrini [a,b,1], A. Dal Lago [c]

[a] Instituto de Astronomía y Física del Espacio, CONICET-UBA, CC 67 Suc. 28, 1428 Buenos Aires, Argentina
[b] Facultad de Ciencias Exactas y Naturales, UBA, Buenos Aires, Argentina
[c] Instituto Nacional de Pesquisas Espaciais, Av.dos Astronautas 1758, 12227-010 São José dos Campos, SP, Brazil

Available online 15 March 2012

Abstract

We revisit previous studies in which the characteristics of the solar and interplanetary sources of intense geomagnetic storms have been discussed. In this particular analysis, using the Dst time series, we consider the very intense geomagnetic storms that occurred during Solar Cycle 23 by setting a value of $Dst_{min} \leqslant -200$ nT as threshold. After carefully examining the set of available solar and *in situ* observations from instruments aboard the Solar and Heliospheric Observatory (SOHO) and the Advanced Composition Explorer (ACE), complemented with data from the ground, we have identified and characterized the solar and interplanetary sources of each storm. That is to say, we determine the time, angular width, plane-of-the-sky, lateral expansion, and radial velocities of the source coronal mass ejection (CME), the type and heliographic location of the CME solar source region (including the characteristics of the sunspot groups), and the time duration of the associated flare. After this, we investigate the overall characteristics of the interplanetary (IP) main-phase storm driver, including the time arrival of the shock/disturbance at 1 AU, the type of associated IP structure/ejecta, the origin of a prolonged and enhanced southward component (B_s) of the IP field, and other characteristics related to the energy injected into the magnetosphere during the storm (*i.e.* the solar wind maximum convected electric field, E_y). The analyzed set consists of 20 events, some of these are complex and present two or more Dst minima that are, in general, due to consecutive solar events. The 20 storms are distributed along Solar Cycle 23 (which is a double-peak cycle) in such a way that 15% occurs during the rising phase of the cycle, 45% during both cycle maxima, and, surprisingly, 40% during the cycle descending phase. This latter set includes half of the superstorms and the only cycle extreme event. 85% of the storms are associated to full halo CMEs and 10% to partial halo events. One of the storms occurred at the time contact with SOHO was lost. The CME solar sources of all analyzed storms, but one, are active regions (ARs). The source of the remaining CME is a bipolar low-field region where a long and curved filament erupts. The ARs where the CMEs originate show, in general, high magnetic complexity; δ spots are present in 74% of the ARs, 10% are formed by several bipolar sunspot groups, and only 16% present a single bipolar sunspot group. All CMEs are associated to long duration events (LDEs), exceeding 3 h in all cases, with around 75% lasting more than 5 h. The associated flares are, in general, intense events, classified as M or X in soft X-rays; only 3 of them fall in the C class, with the one happening in the bipolar low field region hardly reaching the C level. We calculate the lateral expansion velocity for most of the CMEs. The values found exceed in all cases but one the fast solar wind speed ($\approx$750 km s^{-1}). The average lateral expansion velocity is 2400 km s^{-1}. The spatial distribution of the solar CME sources on the solar disk shows an evident asymmetry; while there are no sources located more eastward than 12° in longitude, there are 7 events more westward than 12°. Nevertheless, the bulk of the solar sources are located near Sun center, *i.e.* at less than 20° in longitude or latitude. Considering the IP structures responsible for a long and enhanced B_s, we find that 35% correspond to magnetic clouds (MCs) or ICME fields, 30% to sheath fields, and 30% to combined sheath and MC or ICME fields. For only one storm the origin of B_s is related to the back compression of an ICME by a high speed stream coming from a coronal hole in the neighborhood of the corresponding CME source region. We have also found that for this particular set of storms

* Corresponding author. Tel.: 54 1147816755; fax: 54 1147868114.
E-mail addresses: natisolsz@hotmail.com (N.S. Szajko), gcristiani@iafe. uba.ar (G. Cristiani), mandrini@iafe.uba.ar (C.H. Mandrini), dallago@dge. inpe.br (A. Dal Lago).
[1] Member of the Carrera del Investigador Científico, CONICET, Argentina.

doi:10.1016/j.asr.2012.03.006

the linear relation between E_y and the storm intensity holds (with a correlation coefficient of 0.73). These results complement and extend those of other works in the literature.

Keywords: Very intense geomagnetic storms; Solar activity; CMEs/ICMEs

1. Introduction

Geomagnetic storms are characterized by a sudden enhancement of the ring electric current circulating around the Earth. This current is mainly transported by protons, oxygen ions, and electrons (in the 10–200 keV energy range) during their drift motion. The ring current is located between 2 and 7 Earth radii (see Gonzalez et al., 1994, and references therein). Due to the orientation of the Earth's magnetic field, when the interplanetary (IP) field reaches the Earth's bow shock with a southward orientation, a reconnection process can take place. This process implies the topological change of oppositely directed magnetic structures that are pushed against each other and allows for the mixing of the ensuing flows. As a result, energetic particles coming from the Sun with the solar wind are free to enter the magnetosphere and, after a period of storage, some are injected into the ring current system. The ring current induces a magnetic field, which opposes the dipolar geomagnetic field at the Earth's surface. The geomagnetic disturbance storm time index, Dst, was introduced as a measure of the ring current magnetic field and, therefore, it can be used to quantify the strength of a geomagnetic storm. The Dst index is calculated from measurements of the horizontal component of the magnetic field recorded at several low-latitude observatories (at ground level) and represents the global horizontal component of the geomagnetic field. Independently of their origin, the disturbances to the geomagnetic field have been studied for more than two centuries (e.g. von Humboldt, 1808; Chapman and Bartels, 1940; Rostoker and Fälthammar, 1967; Gonzalez et al., 1994; Tsurutani et al., 1997).

It is now well established that major geomagnetic storms are the consequence of a sequence of events that originate in the Sun and result in a geoeffective solar wind flow near Earth (see examples in Brueckner et al., 1998; Webb et al., 2000; Dal Lago et al., 2004a; Gopalswamy et al., 2005; Harra et al., 2007; Dasso et al., 2009; Rodriguez et al., 2009; Chandra et al., 2010). Broadly speaking, the geoeffective solar wind disturbances can be separated in two types. One of them is associated to IP coronal mass ejections (ICMEs). ICMEs are the counterparts of CMEs in the IP medium. The definition of an ICME is based on several criteria depending on the author and, thus, there is some freedom in their characterization (see e.g. Gosling et al., 1973; Borrini et al., 1982; Gosling et al., 1987; Wang et al., 2005; Liu et al., 2005). However, within ICMEs a particular subset, called magnetic clouds (MCs), fulfills more stringent criteria such as: a smooth and large rotation of the magnetic field vector, a field intensity larger than the surrounding IP field, a low proton temperature, and a low proton plasma β (rate of the proton to the magnetic pressure) (Burlaga et al., 1981; Klein and Burlaga, 1982). The other type of geoeffective solar wind disturbance is associated to the fast solar wind coming from solar coronal holes; this flow interact with the preceeding slow solar wind in zones called corotating interaction regions (CIRs). Several recent works have found that major geomagnetic storms may be driven by either ICMEs/MCs or CIRs (see Echer et al., 2008b, and references therein). However, regardless its solar origin, the geoeffective solar wind flow should be accompanied by a long period of enchanced southward directed IP magnetic field (B_s) to allow for an efficient energy injection into the Earth's magnetosphere and, thus, a storm (Gonzalez et al., 1994). Such period of time can occur at the front or back of an ICME, MC or CIR (see Echer et al., 2008b, and references therein).

According to their $\mathrm{Dst_{min}}$ value, major geomagnetic storms can be classified as: intense, those for which $\mathrm{Dst}_{min} \leqslant -100$ nT (Gonzalez et al., 1994), super intense, when $\mathrm{Dst}_{min} \leqslant -250$ nT (Tsurutani et al., 1992; Gonzalez et al., 2002; Echer et al., 2008a,b; Cid et al., 2008), or extreme, events for which $\mathrm{Dst}_{min} \leqslant -400$ nT (Gonzalez et al., 2011a). The latest are very uncommon, only five extreme storms have been registered since 1957 (see Table 2 in Gonzalez et al., 2011b). During Solar Cycle 23, 11 events were classified as superstorms and only one qualified as an extreme storm.

Solar Cycle 23 is unique in the sense that it is the first of the space age during which the Sun has been imaged almost continuously. The Large Angle and Spectrometric Coronagraph (LASCO, Brueckner et al., 1995), on board the Solar and Heliospheric Observatory (SOHO), has provided a long-term set of observations of coronal mass ejections (CMEs) for which several characteristic parameters have been catalogued in a comprehensive data base (http://cdaw.gsf.nasa.gov/CME_list/, Gopalswamy et al., 2009). The combination of LASCO data with observations from other SOHO instruments, such as the Extreme-ultraviolet Imaging Telescope (EIT, Delaboudiniere et al., 1995) and the Michelson Doppler Imager (MDI, Scherrer et al., 1995), allows us to determine the solar CME source region and its magnetic characteristics. In addition to this, the plasma and magnetic field experiments on board the Advanced Composition Explorer (ACE) and Wind give the opportunity of full *in situ* data coverage in the same

period of time. This combination of observations has motivated various statistical studies concerning the solar and IP origin of major storms for their obvious implications on space weather prediction. In particular, we refer the reader to the work by Zhang et al. (2007), and references therein, for a statistical global analysis of solar and IP sources of intense geomagnetic storms, as well as, to the comprehensive paper by Echer et al. (2008b), and references therein, for a statistical analysis of the IP origin of intense storms. Due to the relevance of the subject and the difficulty of establishing clear one to one associations between solar, IP events, and geomagnetic storms, in this paper we revisit in a systematic way previous statistical works by selecting only the very intense storms (those for which $Dst_{min} \leqslant -200$ nT) that occurred during Solar Cycle 23. For each storm we determine the time, angular width, plane-of-the-sky, lateral expansion, and radial velocities of the source CME, the type and heliographic location of the CME solar source region (including the characteristics of sunspot groups), and the time duration of the associated flare. After this, we investigate the overall characteristics of the IP main-phase storm driver including the time arrival of the shock/disturbance at 1 AU, the type of associated IP structure/ejecta, the origin of a prolonged and enhanced southward component (B_s) of the IP field, and other characteristics related to the energy injected into the magnetosphere during the storm (*i.e.* the solar wind maximum convected electric field, E_y). Our analysis, thus, complements and extends those of other works in the literature.

The outline of this paper is as follows: Section 2 presents the geomagnetic data and the selection criteria, Section 3 refers to the solar sources associated to each geomagnetic event and the methodology that allows us to relate these phenomena, in Section 4 we identify and characterize the IP source that triggers each storm. Finally, in Section 5, we summarize and discuss the results of this work.

2. Geomagnetic data and selection criteria

We use the Dst final values from the World Data Center for Geomagnetism (http://wdc.kugi.kyoto-u.ac.jp/dstdir/index.html) to select the events in our set. The temporal extension of Solar Cycle 23 was taken from October 1996 to December 2008 (see *e.g.* http://www.ips.gov.au/solar). The hourly averaged Dst data are analyzed and plotted to select storms for which $Dst_{min} \leqslant -200$ nT. We found 19 cases that comply with our selection criterion and one case for which $Dst_{min} = -197$ nT. Taking into account that the data are averaged over one hour, we have decided to include this marginal case in our set. Table 1 shows all the selected events. The columns in the table are the event number, the date and time when Dst reached its minimum value and the corresponding Dst_{min} value.

The development of a typical geomagnetic storm related to an ICME and its shock can be described as follows: i) a sudden storm commencement, characterized by a vigorous Dst enhancement due to the compression of the magnetosphere by the shock wave impinging on the Earth's field, ii) a main phase during which Dst decreases as a response to the ring current increase, iii) a recovery phase that can last up to several days, characterized by a decay of the ring current due to a combination of different energy loss mechanisms (e.g. Fok et al., 1995). Several of the storms in our set follow the previous description and display a single minimum during their development; however, some have more complex Dst profiles with several consecutive minima. If during a period of strong solar activity we observe multiple Dst values $\leqslant -200$ nT, we assign them to different geomagnetic storms if we are able to identify both their solar origin and the IP cause of B_s. This is the case for events number 13 and 14 and 17 and 18 that are separated in time by almost one day and more than two days, respectively. Events 8 and 9 seem to consitute a two-step single geomagnetic storm, as we will discuss in Section 4; however, we will keep them as separated events in this table. During Solar Cycle 23, most of the storms showing these characteristics occurred either during solar maximum or during the "Halloween" time in October–November 2003 (see Gopalswamy et al., 2005, for a global description of the extreme solar activity in this period).

Table 1
Very intense geomagnetic storms during Solar Cycle 23.

#	Date and time Dst_{min}	Dst_{min} (nT)
1	04 May 1998-05:00 UT	−205
2	25 Sep 1998-09:00 UT	−207
3	22 Oct 1999-06:00 UT	−237
4	06 Apr 2000-23:00 UT	−287
5	16 Jul 2000-00:00 UT	−301
6	12 Aug 2000-09:00 UT	−235
7	17 Sep 2000-23:00 UT	−201
8	31 Mar 2001-08:00 UT	−387
9	31 Mar 2001-21:00 UT	−284
10	11 Apr 2001-23:00 UT	−271
11	06 Nov 2001-06:00 UT	−292
12	24 Nov 2001-16:00 UT	−221
13	30 Oct 2003-00:00 UT	−353
14	30 Oct 2003-22:00 UT	−383
15	20 Nov 2003-20:00 UT	−422
16	27 Jul 2004-13:00 UT	−197
17	08 Nov 2004-06:00 UT	−373
18	10 Nov 2004-10:00 UT	−289
19	15 May 2005-08:00 UT	−263
20	24 Aug 2005-11:00 UT	−216

Fig. 1 show, at the top, the distribution of the intensity of the analyzed events and, at the bottom, their occurrence rate per year. If we consider the classification discussed in Section 1, we see that 60% of all the very intense storms of Cycle 23 were super intense storms (or superstorms), including an extreme event. More surprising is the distribution of these very intense storms along the solar cycle. Solar Cycle 23 was a clearly double-peak cycle, with one maximum in 2000 and a second one in 2002 (see Fig. 1, bottom). Fig. 1 (bottom) shows that 15% of the events occurred during the cycle rising-phase. All these events are very intense storms. During the first cycle maximum the number of very

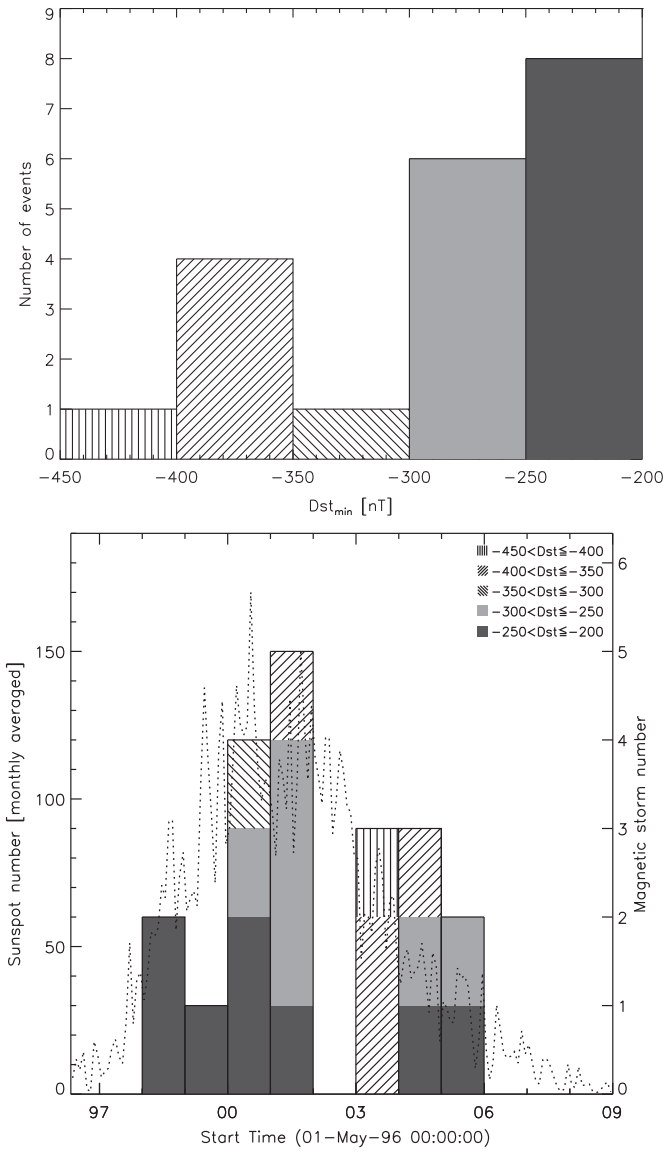

Fig. 1. Top: Histogram showing the distribution of Dst_{min} for very intense geomagnetic storms (in 50 nT bin sizes). Bottom: Storm occurrence rate per year (vertical left-hand axis). The overlaid dotted line shows the monthly averaged sunspot numbers, as indicated in the right-hand vertical axis. In both figures, different shadings and hatchings correspond to Dst_{min} values separated in 50 nT ranges. The storm with $Dst_{min} = 197$ nT will be included, from now on, in the set that ranges between-250 and-200 nT.

intense storms increased to 20%. During the second cycle maximum it reached 25% with all of them, but one, being superstorms. However, half of all superstorms (6), including one extreme event, occurred during the cycle descending phase.

3. The solar sources: CMEs and their origin at the Sun

To identify the solar source event and the region from which it originates at Sun's surface, we have proceeded by tracking the possible solar candidate from Sun to Earth and, in several ambiguous cases, back from Earth to Sun, as we discussed below.

We have predominantly used observations from instruments aboard SOHO. These data are available at the time of 19 out of the 20 analyzed events; one of the events in our list occurred when contact with SOHO was lost. During Solar Cycle 23, CMEs have been mostly seen near the Sun by LASCO C2 and C3 coronagraphs that cover the range from ≈2 to 30 solar radii measured from Sun center. We have extensively used LASCO data base at http://cdaw.gsf.nasa.gov/CME_list/. The location and characteristics of the event on the Sun are determined using mainly EIT observations in the 195 Å passband, which are the ones in EIT data base with the largest temporal coverage. We have also used data in other passbands, *e.g.* 171 Å and 304 Å, in particular, the daily movies at http://www.ias.u-psud.fr/eit/movies/. These data are complemented with magnetic and white light observations from MDI data base (http://soi.stanford.edu/data/), that we use to characterize the degree of magnetic complexity of the region. The class, both in soft X-rays (1-8 Å) and Hα, and duration of the flares associated to the CMEs are taken from Solar Geophysical Data (SGD) reports or directly from the Geostationary Operational Environmental Satellites (GOES) data base, when we find some inconsistency in the determination of the flare duration. We have also used data from ground based observatories, in particular, Hα observations from public data bases (*e.g.* http://bass2000.obspm.fr/home.php).

Our procedure to identify the solar source event is as follows. We first consider a time window between 24 h (transit CME speed from Sun to Earth ≈1800 km s^{-1}) and 120 h (transit CME speed ≈350 km s^{-1}) previous to the geomagnetic event to select a candidate CME. This time window roughly takes into account the range of plausible CME speeds measured in coronagraph data. In order to decrease the possible number of candidates, we first consider only frontside full halo CMEs and, in a second step, partial halo CMEs with a large "apparent" angular width (AW $\geqslant 150^{\circ}$). We do so because the source region of a geoeffective solar event is expected to be close to disk center. This implies a large angular width, attributed both to projection effects and to a large intrisic width, indicating that the CME is likely directed along the Sun-Earth line. Nevertheless, there are exceptions to a central disk location with extreme cases being launched at the limb or even in the Sun's back side (Zhang et al., 2003). We then use the CME speed reported in LASCO catalogue by a second order fitting to C2 and C3 observations to identify by forward timing (from Sun to Earth) the possible solar source candidate.

The previous discussed search does not provide, in general, a one-to-one correspondence; more than one solar CME can be linked to a particular geomagnetic storm. Therefore, to further constrain our search, we estimate the CME transit time (backward timing, from Earth to Sun) using the solar wind radial velocity of the IP structure identified as source of B_s (v_{sr} in Table 3, see Section 4). We proceed in this way because, as indicated in several reviews

Table 2
CMEs and their source ARs associated to the very intense storms of Solar Cycle 23.

#	Active region		Flare			CME				
	AR location	Sunspot group	X-ray t_{max}	Importance X-ray/opt.	Durat. (h)	Lasco C2	Type	v (km/s)	v_{exp} (km/s)	v_{re} (km/s)
1	AR8210 (S15W15)	$\gamma\delta$	02 May 98-13:42 UT	X1.1/3B	5.23	02 May 98-14:06 UT	HALO	697	1228	1081
2	AR8340 (N20E09)	β	23 Sep 98-07:13 UT	M7.1/3B	16.16	No data[a]				
3	No AR[b](S20E05)	QS	17 Oct 99-23:22 UT	C1.2/ND	3.70	18 Oct 99-00:06 UT	PH(AW=240)	263	546	480
4	AR8933 (N16W66)	β	04 Apr 00-15:41 UT	C9.7/2 F	5.22	04 Apr 00-16:32 UT	HALO	1232	1927	1696
5	AR9077(N22W07)	$\beta\gamma\delta$	14 Jul 00-10:24 UT	X5.7/3B	4.60	14 Jul 02-10:54 UT	HALO	1534	2178	1917
6	AR9114(N11W11)	$\beta\gamma$	09 Aug 00-16:22 UT	C2.3/SF	5.18	09 Aug 00-16:30 UT	HALO	731	898	790
7	AR9165(N14W07)	$\beta\delta$	16 Sep 00-04:26 UT	M5.9/2B	4.23	16 Sep 00-05:18 UT	HALO	1162		
8	AR9393(N16W10)[c]	$\beta\gamma\delta$	29 Mar 01-10:15 UT	X1.7/1 N	3.78					
	29 Mar 01-10:26 UT		965	1511	1330					
9	AR9393(N18E02)		28 Mar 01-12:40 UT	M4.3/SF	3.83	28 Mar 01-12:50 UT	HALO	582		
10	AR9415(S21W04)	$\beta\gamma\delta$	09 Apr 01-15:43 UT	M7.9/2B	5.00	09 Apr 01-15:54 UT	HALO	1198	2679	2358
11	AR9684(N06W18)	$\beta\gamma$	04 Nov 01-16:20 UT	X1.0/3B	9.95	04 Nov 01-16:35 UT	HALO	1514	3670	3230
12	AR9704(S10W39)	$\beta\gamma\delta$	22 Nov 01-23:30 UT	M9.9/3B	8.53	22 Nov 01-23:30 UT	HALO	1371	2800	2464
13	AR10486(S16E08)	$\beta\gamma\delta$	28 Oct 03-11:10 UT	X17/4B	11.16	28 Oct 03-11:30 UT	HALO	2229	4800	4224
14	AR10486(S15W02)	$\beta\gamma\delta$	29 Oct 03-20:49 UT	X10/2B	5.28	29 Oct 03-20:54 UT	HALO	1670	4000	3520
15	AR10501(N03E08)	$\beta\gamma\delta$	18 Nov 03-08:31 UT	M3.9/2 N	8.42[d]	18 Nov 03-08:50 UT	HALO	1645	2900	2552
16	AR10652(N08W33)	$\beta\gamma\delta$	25 Jul 04-15:14 UT	M1.1/ND	6.68	25 Jul 04-15:14 UT	HALO	1366		
17	AR10696(N10E08)	$\beta\gamma\delta$	06 Nov 04-00:34 UT	M9.3/2 N	6.90	06 Nov 04-02:06 UT	PH(AW=214)	1111	1562	1375
			06 Nov 04-00:57 UT	M5.9/ND						
			06 Nov 04-01:57 UT	M3.6/ND						
18	AR10696/AR10695 (N10W10)[e]	$\beta\gamma\delta/\beta$	07 Nov 04-16:06 UT	X2.0/ND	8.16	07 Nov 04-16:54 UT	HALO	1696	3077	2708
19	AR10759(N12E12)	β	13 May 05-16:57 UT	M8.0/2B	12.78	13 May 05-17:22 UT	HALO	1690		
20	AR10798(S16W70)	$\beta\gamma\delta$	23 Aug 05-14:44 UT	M2.9/SF	9.70	23 Aug 05-14:54 UT	HALO	2123	3100	2728

[a] No LASCO data from July to September 1998. ND in the fifth column means no Hα data.
[b] Low intensity bipolar region where a filament eruption occurs (see text).
[c] Location of AR9393 at the time when two CMEs that could be the source of the two-step storm (events 8 and 9) occurred.
[d] This duration corresponds to two consecutives flares in AR10501, one on 18 Nov 2003-07:52 UT (M3.2/2 N) and the one included in the table.
[e] The halo CME that resulted in storm number 18 is related to the interaction between AR10695 and AR10696. The heliographic coordinates in this column are those of AR10696.

Table 3
Interplanetary structures that gave rise to very intense geomagnetic storms during Solar Cycle 23.

#	Shock/disturbance	IP structure	B_s origin	v_{rs} (km/s)
1	04 May 98-02:10 UT	ICME	sheath	780
2	24 Sep 98-23:15 UT	ICME/MC	sheath+MC	800
3	21 Oct 99-01:34 UT	ICME	back compression ICME	500
4	06 Apr 00-16:02 UT	ICME	sheath	680
5	15 Jul 00-14:18 UT	ICME/MC	MC	800
6	11 Aug 00-18:19 UT	ICME/MC	sheath+MC	650
7	17 Sep 00-17:00 UT[a]	ICME/MC	MC	800
8	31 Mar 01-00:14 UT[b]	ICME/MC?	sheath+MC?	700
9			MC?	
10	11 Apr 01-15:18 UT	ICME/MC	sheat+MC	750
11	05 Nov 01-16:30 UT[a]	ICME	sheath	400
12	24 Nov 01-05:30 UT	ICME/MC	sheath	900
13	29 Oct 03-06:00 UT	ICME/MC	MC	1500
14	30 Oct 03-16:10 UT	ICME/MC	sheath	1300
15	20 Nov 03-07:20 UT	ICME/MC	MC	720
16	26 Jul 04-20:00 UT	ICME/MC	sheath+MC	900
17	07 Nov 04-18:00 UT	ICME/MC?	MC?	720
18	09 Nov 04-18:20 UT	ICME/MC	sheath+MC	800
19	15 May 05-02:00 UT	two MCs	MC	900
20	24 Aug 05-05:30 UT	ICME	sheath	600

[a] The presence of a shock is not clear.
[b] See text for a discussion on the geoeffective IP structures for this two-step storm. When an interrogation mark is indicated by the letters MC, it means that the cloud signatures are marginal.

that discuss the association between CMEs and ICMEs (e.g. Démoulin, 2008), this velocity is closer to the transit speed from Sun to Earth when considered as constant. Since fast CMEs tend to decelerate when travelling in the slower solar wind, this will give an upper estimate for the transit time. For slow CMEs this method is not useful, as initially slow CMEs may be accelerated by the ambient solar wind. To these timings, we also add the consideration of the CME solar source location given by the eruptive features observed in EIT images, *i.e.* flare brightenings, post-flare arcades, or coronal dimmings (see Attrill et al., 2006, and references therein). We favour sources located close to disk center with respect to near-limb sources, though, as mentioned before, this is not a severe constraint. The combination of these procedures has allowed us to associate a CME to a selected storm and even to each value of $\mathrm{Dst_{min}} \leqslant -200$ nT, when two are found within a time difference of around one day. We show an example of such an association in Fig. 2. Our results show that 85% of the storms in our set are associated to full halo CMEs and 10% to partial halos with an AW $\geqslant 200^{\circ}$. The remaining storm occurred when contact with SOHO was lost.

Once the source CME and the location on the Sun from which it originates are determined, we identify the AR, the class (in soft X-rays and Hα) and duration of the associated flare using SGD reports and GOES data, and the degree of magnetic complexity of the AR using MDI data. The flare duration is taken from the time of impulsive soft X-ray increase to the time when the flux returns either to its pre-flare level or another flare occurrs in a different or the same AR, being clearly distinguishable from the CME associated flare. All these characteristics are listed in Table 2, in which: the first column corresponds to the number of event as in Table 1, the second column gives the AR NOAA number and its heliographic location, the third column corresponds to the standard sunspot group classification at the time of CME occurrence, the fourth column gives the time of maximum soft X-ray flux for the associated flare from which the X-ray classification is derived (this is shown together with the Hα class in the fifth column), the sixth column corresponds to the flare duration computed as already discussed, the seventh, eigth, and ninth columns provide information from the LASCO CME catalogue and show the time of first appearance in C2, the CME type, and its velocity (second order fitting to C2 and C3 data). We have also added the CME lateral expansion and radial velocities that we determine as discussed in the next paragraph.

The CME speed projected on the plane-of-the-sky (v in Table 2) does not represent the real CME earthward directed speed. In order to estimate the radial Sun-Earth speed, v_{re}, we first calculate the CME lateral expansion velocity (v_{exp}) and apply the phenomenological relation found by Dal Lago et al. (2003) to infer its value. The relation between these velocities is $v_{re} = 0.88 v_{exp}$. The method to compute the CME lateral expansion velocity for limb and partial halo CMEs is described in Dal Lago et al. (2003), while Dal Lago et al. (2004b) do it for full halo CMEs. The v_{exp} values are listed in the tenth column of Table 2, while its eleventh column shows those of v_{re}. Rows without data in columns 10 and 11 indicate that there are not enough data points in C2 and C3 fields of view for a reliable determination of v_{exp}. The average lateral expansion velocity value is 2400 km s^{-1}. In all cases, v_{re} is much

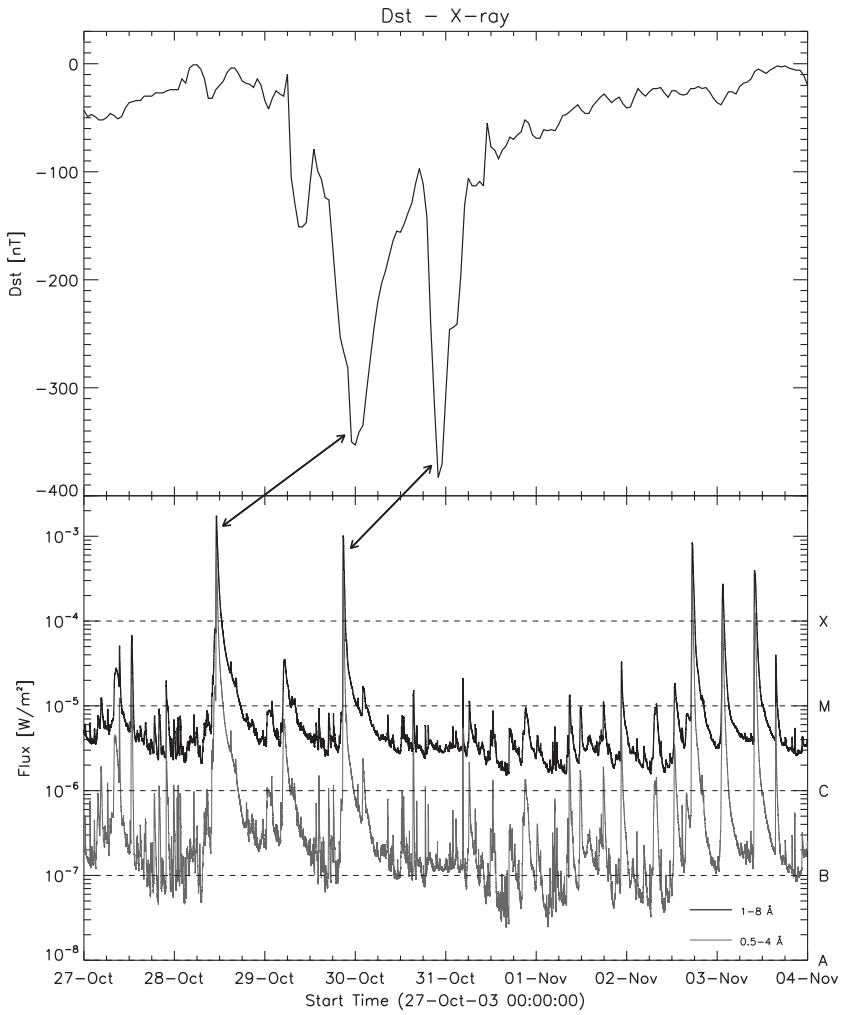

Fig. 2. GOES light curve in 1-8 Å for the solar flares on 28 and 29 October 2003 (bottom) and the associated geomagnetic storms (top), events 13 and 14 in Table 1.

higher than the projected plane-of-the-sky velocity, indicating that CMEs can be much faster when leaving the Sun and up to a distance equivalent to ≈30 solar radii. It is also evident, when v_{re} is compared to v_{rs} in Table 3, that all fast CMEs are strongly decelerated during their transit to 1 AU; while slow CMEs (see *e.g.* event number 3) are accelerated by the ambient solar wind, as previously discussed.

The CME solar sources of all analyzed storms, but one, are ARs. The source of the remaining CME is a bipolar low-field region. A long and curved filament lies along the polarity inversion line in this region and extends in the quiet Sun (QS), between its trailing polarity and the leading polarity of a nearby decayed region to the east. This filament erupts on 17 October 1999 at around 23:20 UT and a partial halo CME is seen in C2 on 18 October at 00:06 UT. The filament is visible in Hα images from Paris Observatory in Meudon on 17 October and has disappeared on the next day. A C1.2 class flare is registered by GOES. The emission in soft X-rays decays to class B after one hour, but the loops in the region continue being bright in EUV until 4:00 UT on 18 October; it is the duration of this emission the one listed in column 6 for this event. Even though this is the weakest flare, it occurs in a spotless low intensity magnetic field region, and the associated CME is the slowest, it produced a very intense storm that reached a $\mathrm{Dst}_{\mathrm{min}} = -237$ nT (see also Dal Lago et al., 2004a).

The ARs where the CMEs originate show, in general, high magnetic complexity; δ spots are present in 74% of the cases, 10% are formed by several bipolar sunspot groups, and only 16% present a single bipolar sunspot group. All CMEs are associated to long duration events (LDEs), exceeding 3 h in all cases, with around 75% lasting more than 5 h. The associated flares are, in general, intense events, classified as M or X in soft X-rays; only 3 of them fall in the C class, with the one discussed in the previous paragraph reaching only class C1.2.

Fig. 3 shows the spatial distribution of the CME source regions on the solar disk. There is an evident asymmetry, while there are no sources located more eastward than 12° in longitude, there are 7 events more westward than 12°. Despite this asymmetry, the bulk of the solar sources

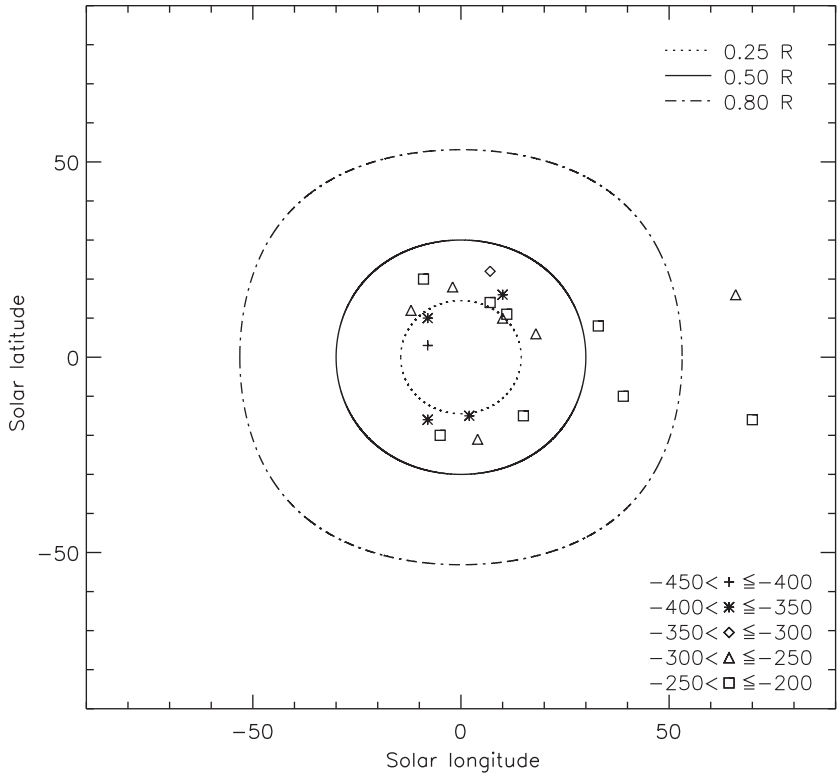

Fig. 3. Heliographic distribution of source regions producing the CMEs that originate very intense storms during Solar Cycle 23 (R stands for the solar radius).

are located near Sun center, *i.e.* at less than 20° in longitude or latitude.

4. The associated interplanetary medium events

Since storms are driven by the solar wind magnetic field and plasma impinging on the Earth's magnetosphere, we use here *in situ* data from instruments aboard ACE to identify the IP structures responsible for each goemagnetic storm. In particular, we have used plasma data from the Solar Wind Electron Proton and Alpha Monitor (SWEPAM, McComas et al., 1998) and magnetic field data from the Magnetic Fields Experiment (MAG, Smith et al., 1998).

Taking into account their magnetic and plasma signatures, we are able to identify various types of structures associated with the very intense geomagnetic storms of Cycle 23. These structures include ICMEs, ICMEs containing a flux tube with MC properties, the sheath between the CME driven shock and the ICME, and regions with clear signatures of interaction between ICMEs and high speed streams from coronal holes. Table 3 lists the results of this association, the first column corresponds to the geomagnetic event number, the second column to the arrival date and time of the shock or disturbance at 1 AU, the third column to the characteristics of the IP structure, the fourth column indicates the origin of the prolonged and enhanced B_s, and the fifth column lists the average radial solar wind velocity (v_{rs}) during the storm main phase. If the IP structure has ICME signatures and no MC characteristics are present within it, we only indicate ICME in column 3, if conversly MC characteristics are present we write ICME/MC.

Fig. 4 illustrate the way we have proceeded in this identification. The plots correspond to the storm with $\mathrm{Dst}_{min} = -263$ nT on 15 May 2005 at 08:00 UT. From top to bottom the figure shows, the IP magnetic field intensity, the southward component of the IP field, the solar wind radial velocity, the proton temperature and density, the proton plasma β parameter, and the geomagnetic storm profile. The presence of a MC is evident from these figures. In fact, the detailed analysis by Dasso et al. (2009) shows that two MCs, that interacted during their travel from the Sun to 1 AU, are present between the second and third vertical dashed-dotted lines. These two clouds are the result of two consecutive eruptions of two portions of the AR region filament that resulted in the longest LDE in the flare list of Table 2. The time between the first and second vertical dashed-dotted lines corresponds to the sheath (between 15 May 02:11 UT and 05:42 UT). After the sheath, a first cloud is observed between 15 May 05:42 UT and 10:20 UT; this structure is evident by the large coherent rotation of B_z that goes from south to north. After this period there is a change in the rotation and discontinuity in the field. The period of time between 15 May 10:20 UT and 14:10 UT has the characteristics of a flux rope back, defined by Dasso et al. (2006). Later, between

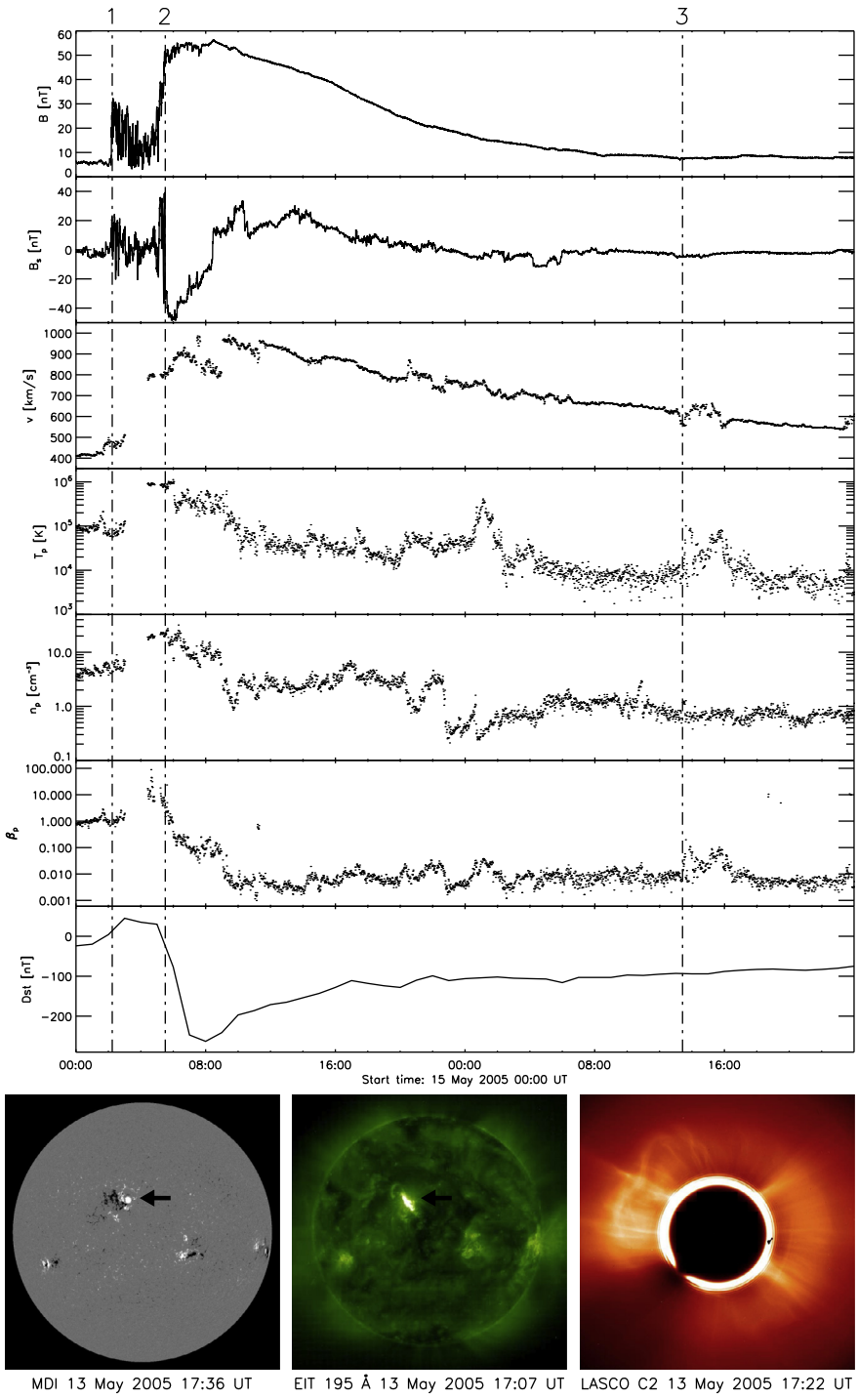

Fig. 4. Interplanetary, geomagnetic, and solar data related to event number 19 in Table 1, $Dst_{min} = -263$ on 15 May 2005 at 08:00 UT. The figure shows, from top to bottom, the IP magnetic field intensity, the southward component of the IP field in GSM coordinates, the solar wind radial velocity, the proton temperature and density, the proton plasma β parameter, and the geomagnetic storm profile. The meaning of the vertical lines is explained in the text. The three images at the bottom illustrate the location of the source AR (pointed with an arrow) in an MDI magnetogram, the EUV flare in EIT, and the LASCO C2 field of view at 17:22 UT.

15 May 14:10 UT and 16 May 04:10 UT (last vertical line in Fig. 4) there is a second very extended structure in which the field rotates coherently, displays a low proton plasma β and (except for a bump in the curve) a low proton temperature. These timings and a magnetic field model and description of the MCs and other IP structures can be found in Dasso et al. (2009). It is clear from the figure that the origin of B_s and, therefore, the cause of the storm is the first MC field. These two interacting MCs produced a single-step storm as they started travelling together, with-

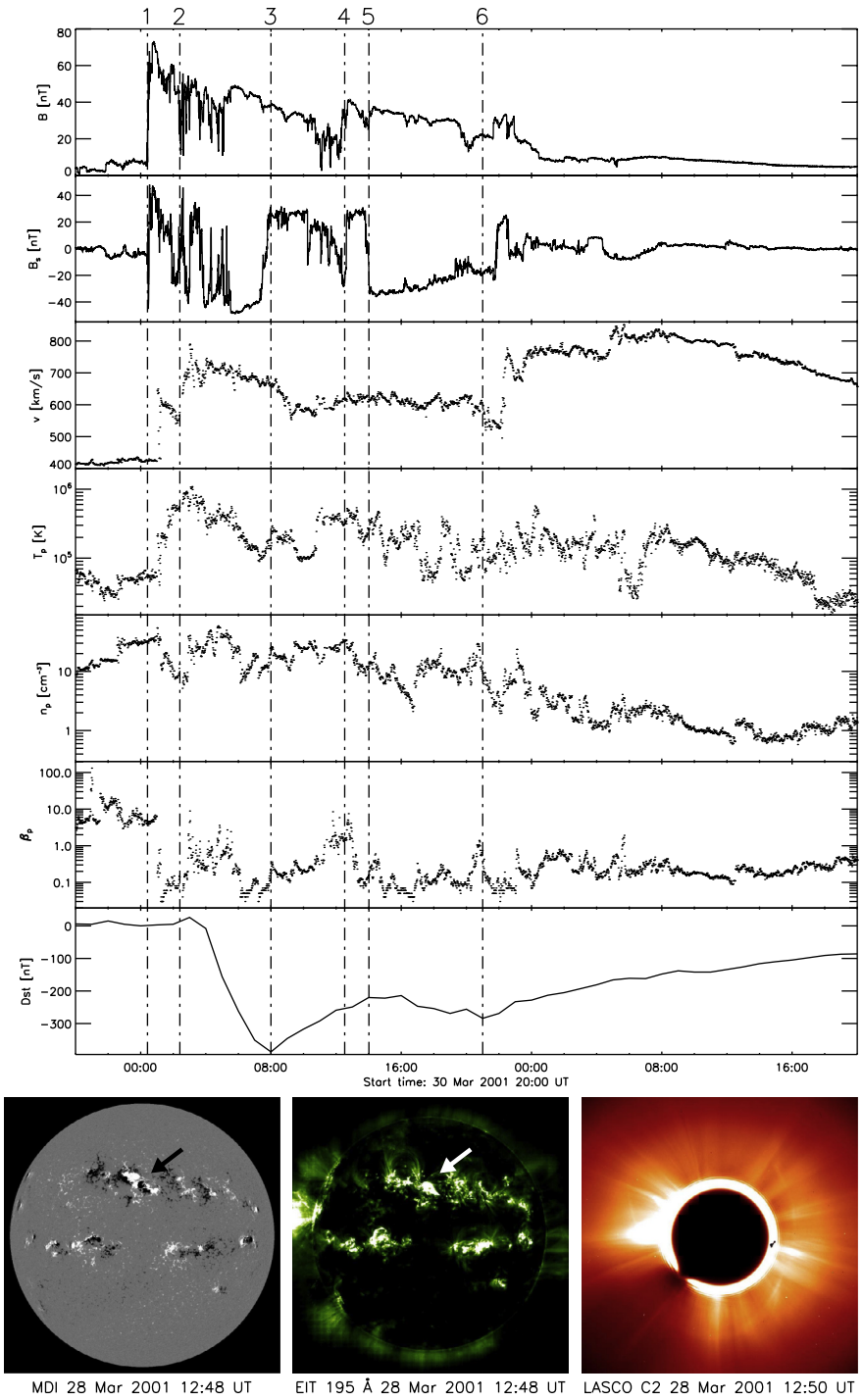

Fig. 5. Same data as on Fig. 4 for event number 8 and 9 in Table 1. The meaning of the vertical lines is explained in the text. The three images at the bottom illustrate the location of the source AR (pointed with an arrow) in an MDI magnetogram, the EUV flare in EIT (pointed with an arrow), and the LASCO C2 field of view at 12:50 UT.

out merging (see the previous mentioned work and also Bisi et al., 2010), preceeded by a single shock as shown in Fig. 12 of Dasso et al. (2009).

In the case of events 8 and 9 from Table 1, we have two solar flares and two associated CMEs, with the second one being faster than the first one. This velocity difference would imply that they encounter in their travel from Sun to Earth, but probably still preserve their own characteristics when arriving at 1 AU. Fig. 5 displays the same IP parameters as Fig. 4. At around 00:15 UT on 31 March 2001, a fast increase of the IP magnetic field is evident. Sheath fields with an average southward component of the IP field (except for a short period of time) are present after 02:24 UT, this time corresponds to the storm

commencement and part of it main phase (for a detailed analysis see Wang et al., 2003). After that and until the first Dst_{min} value, ICME fields are responsible for B_s. Though a clear smooth and long rotation of the field is seen until around 12:31 UT, accompanied by a low proton plasma β value, the proton temperature stays high; that is why, we have added a question mark by the letters MC in Table 3, as one requesite for this structure to be a MC is missing. A magnetic discontinuity is present at that time and the proton plasma β increases, to decrease later. An enhanced magnetic field is present after this discontinuity with a southward component of the field starting at 14:01 UT and until after the second Dst_{min}, at around 21:00 UT. Although the first shock sheath and ICME B_s field caused the first deepest Dst_{min}, it is possible that a second ICME may have interacted with the first one and played a role in this event causing the second Dst_{min} during this two-step storm. The IP magnetic field evolution shown in Fig. 4, together with the Dst profile during this complex geomagnetic storm, are fully compatible with those derived from the numerical simulations of Xiong et al. (2009) (see also Xiong et al., 2007) for the interaction of two ICMEs during their transit from Sun to Earth.

Empirical studies of geomagnetic storms, in general, have shown that their primary IP cause is the dawn-to-dusk electric field associated to the passage of a southward B_s field (Gonzalez et al., 1994). To investigate this for the set very intense storms during Solar Cycle 23, we study the correlation between the maximum convected electric field (E_y) during the storm main phase and the Dst_{min} value. The average solar wind radial velocity (v_{sr}), during the storm main phase, has been used together with the B_s peak value to obtain an estimate of the maximum E_y value for each storm. Fig. 6 shows the corresponding scatter plot. A linear relation with a correlation coefficient of 0.73 holds, indicating that, as for geomagnetic storms in general, the physical mechanism behind the cause of very intense ones seems to be associated to the dawn-to-dusk electric field.

Considering the IP structures responsible for a long and enhanced B_s, from Table 3, we find that 35% corresponds to magnetic clouds (MCs) or ICME fields, 30% to sheath fields, and 30% to combined sheath and MC or ICME fields. This latter type of storms shows a two-step development of their main phase, being the first Dst_{min} value related to the B_s sheath field, followed by a partial recovery short period and a more intense Dst minimum related to the MC or ICME B_s field. However, see the description of events 8 and 9 in the previous paragraph. Event number 3 is the only one for which the origin of B_s is related to the back compression of an ICME by a high speed stream coming from the coronal hole in the neighborhood of the CME source region (see a detailed analysis in Dal Lago et al., 2006). This is the storm whose solar origin is a weak and spotless magnetic region. Compared to all our examples, this event is peculiar both for its solar and IP origin.

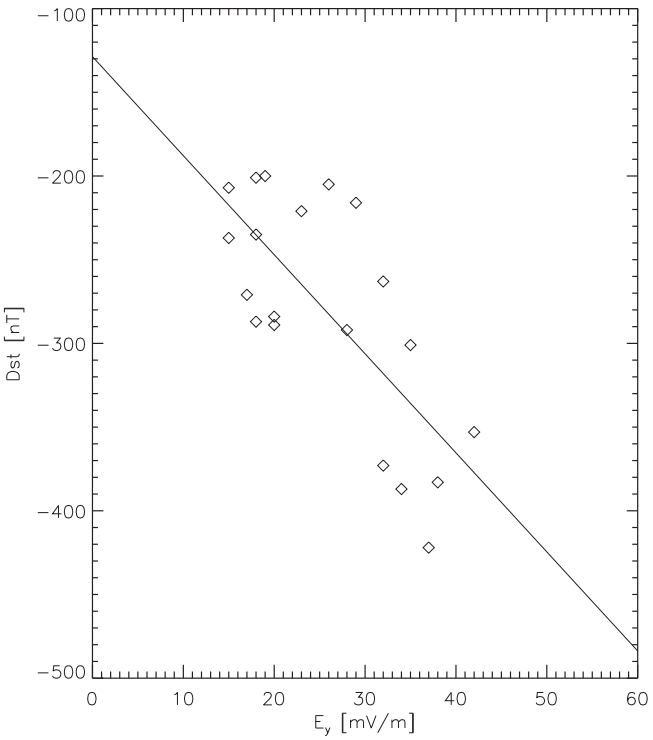

Fig. 6. Correlation between Dst_{min} and the maximum electric field convected by the solar wind (E_y).

5. Summary and discussion

We have analyzed the full set of very intense geomagnetic storms that occurred during Solar Cycle 23 in search of their solar and interplanetary origin.

Our results globally agree with those of previous statistical works such as those by Zhang et al. (2007), and references therein, and Echer et al. (2008b), and references therein. However, there are some differences in the interpretation of the origin of some of the events. In our analysis we have computed the expansion and radial velocities of the source CME and several characteristics of the CME source region and associated flare. We have also profit from our own analysis of particular cases (Dal Lago et al., 2004a; Dal Lago et al., 2006; Harra et al., 2007; Dasso et al., 2009; Mandrini et al., 2007; Chandra et al., 2010) to further constrain our results.

When we investigate the distribution of very intense storms along Solar Cycle 23, which was double peaked, we see that 15% of the events occurs during the cycle rising-phase. All these events are very intense storms. During the first cycle maximum, the number of very intense storms increases to 20%. During the second cycle maximum, it reaches 25% with all of them, but one, being superstorms. However, 40% of the very intense storms with half of all superstorms (6), including one extreme event, occurs during the cycle descending phase. These results, then, show that the distribution of very intense storms, as that of intense storms along the cycle (see Echer et al., 2008b; Gonzalez et al., 2011b, and references therein) presents

two peaks: one during cycle maximum and another one during the descending phase. These results have been presented in a very recent paper by Gonzalez et al. (2011b) (and references therein). These authors have put into historical context all superstorms and extreme events of the space era.

Being the conditions at the Sun the ultimate cause of major geomagnetic disturbances, the question now arises about the existence of those peaks. The presence of the first peak is, in principle, related to the presence of a larger number of ARs on the solar disk implying, then, a higher probability for the occurrence of solar active events, a subset of which will be geoeffective. However, the peak during the descending phase may be related, not to the number of ARs (as this is decreasing), but to other characteristics. For Solar Cycle 23, the 6 superstorms (with one exteme event) in this phase occur during 2003, 2004, and 2005. The associated solar flares/CMEs in 2003 originated from the most complex and intense field AR (AR10486) during the time period of the famous "Halloween" events, and from the only notorious complex region on the Sun (AR 10501) in November, that was the return of the previous solar rotation AR 10484 (see Mandrini et al., 2006; Mandrini et al., 2007; Chandra et al., 2010, for an analysis and modelling of the solar events and associated MC). The latter is the source to the solar flare/CME producing the extreme storm. The associated solar flares/CMEs in 2004 are all related to the only highly magnetically complex AR (AR10696) seen in November, that during one of the events interacted via reconnection (accompanied by the formation of transequatorial loops) with a decayed region in the opposite solar hemisphere (AR10695) (see Harra et al., 2007). The superstorm in 2005 is associated to the only very intense field region on the Sun at that time, AR 10759. Though this AR is bipolar, its complexity derives from the emergence of several bipoles with the same field orientation, which resulted in a very extended and curved magnetic inversion line (see Dasso et al., 2009, and Fig. 4). Then, it seems that, though the number of ARs is decreasing, this stage of the solar cycle is characterized by the presence of some very complex and intense field regions. Furthermore, it is worth recalling the case AR 7978, called the "the last best old-cycle region" by Hudson et al. (1998), that by the end of Solar Cycle 22 was the only sizeble AR on the solar disk during five solar rotations (July 1996–November 1996). This AR produced 26 visible CMEs during its lifetime (van Driel-Gesztelyi, 1998; Démoulin et al., 2002; Mandrini et al., 2004). It is, then, worth investigating, and we propose to do so, if this is also the case for all preceeding cycles for which magnetic field observations are available. The results of such an analysis should set constraints on solar dynamo models.

All CME sources of the IP disturbances causing very intense geomagnetic storms are either full halo CMEs or partial halos with a large angular width as, in principle, expected. The calculated average lateral expansion velocity of the CMEs is $\approx$2400 km s^{-1}. In all cases, the derived Sun-Earth line velocity is much higher than the projected plane-of-the-sky speed. All the observed CMEs, but one, are really fast events with radial velocities reaching 4000 km s^{-1} with an average value of $\approx$2200 km s^{-1}. It is also evident from our analysis that all fast CMEs are strongly decelerated during their transit to 1 AU, while slow CMEs (see *e.g.* event number 3) are accelerated by the ambient solar wind.

The CME solar sources of all analyzed storms, but one, are ARs. The ARs where the CMEs originate show, in general, high magnetic complexity (see the discussion above); δ spots are present in 74% of the cases, 10% are formed by several bipolar sunspot groups, and only 16% present a single bipolar sunspot group. This is not surprising as it is well-known that ARs contaning δ spots display a high level of activity (see Zirin and Liggett, 1987; Poisson et al., 2011). Numerical simulations of magnetic flux emergence (Linton et al., 1998; Fan et al., 1999; Fan, 2009) suggest that δ spots could be the manifestation of the emergence of magnetic flux tubes that have been deformed by the development of a kink instability. Such a magnetic configuration is related to a high degree of magnetic twist. This twist transfers from the field lines that form the main magnetic flux tube, representing the AR, to its axis; therefore, such configurations imply a high magnetic free energy content. The source of only one CME is a low-field region where a long and curved filament erupted. The consequent CME has a propagation direction considerably out of the Sun-Earth direction, it is the slowest, and its associated flare is the less intense. However, this event produced a very intense storm ($Dst_{min} = -237$ nT). At the IP, the ICME was compressed from behind by a high speed stream coming form a near by coronal hole, clearly visible in the Soft X-ray Telescope (SXT, Tsuneta et al., 1991) images aboard the *Yohkoh* satellite (see http://ylstone.physics.montana.edu/ylegacy/). It is probably this compression that makes the IP magnetic field raise in intensity (in particular, its southward directed component) at the back of the ICME, thus, increasing its geoeffectivenes.

All CMEs are associated to LDEs, exceeding 3 h in all cases, with around 75% lasting more than 5 h. The associated flares are, in general, intense events, classified as M or X in soft X-rays; only 3 of them fall in the C class. LDEs are strongly linked to classical two-ribbon flares, which develop after filament eruptions (see Sheeley et al., 1983; Webb and Hundhausen, 1987). The brightenings in these flares are connected by flare loops, which represent field lines reconnected in the current sheet formed in the wake of the erupting filament. This ongoing reconnection process lasts several hours and, therefore, it is not surprinsing that all our events are associated to LDEs, which have a strong link to CMEs (see also Feminella and Storini, 1997).

When we look for the location of the CME source regions producing very intense storms, we find that 75% are located at a distance smaller than half a solar radius (see Fig. 3) (one flare/CME is not observed by SOHO). If we separate this restricted set in Dst_{min} ranges, the ones

in the ranges with lower absolute values have source regions at larger distances from Sun center. In four of these cases the AR is closer to the western limb, with two events at a longitude $\leqslant 60°$. As indicated previously by Wang et al. (2002); Zhang et al. (2003); Zhao et al. (2006); and Zhang et al. (2007) for different sets of analyzed data, there is a a remarkable east-west assimetry in the geoeffective-CME distribution. In a strict sense, our results show that there are more western than eastern CMEs associated to very intense storms since as shown by Cane et al. (2000) and Wang et al. (2002) Earth-impacting CMEs are uniformly distributed in longitude over the solar disk. The origin of this assymetry has been discussed and modelled by Siscoe et al. (2007). These auhtors showed that the effect of the prevailing Parker spiral orientation of the field on the draping of the sheath around the ICME body could account for the greater geoeffectiveness of west hemisphere CMEs compared with east hemisphere CMEs.

Finally, considering the IP structures responsible for a long and enhanced B_s, we find that 35% are MCs or ICME fields, 30% sheath fields, and 30% combined sheath and MC or ICME fields. Therefore, for this particular set, any of these structures is equally important. We have found no storm originated by CIR fields, only one storm is related to the compression of an ICME by a high speed stream coming from a coronal hole. Strictly speaking, this is not a CIR as it is not a region of interaction between the slow and the fast solar wind. We have also found that the linear relation between the maximum value of E_y and the storm intensity holds (with a correlation coefficient of 0.73). No correlation is found with B_s or v_{rs} separately and $\mathrm{Dst}_{\min}$. More stringent criteria, as that propose by Gonzalez and Tsurutani (1987), have been tested by Echer et al. (2008b), see also Ontiveros and Gonzalez-Esparza (2010).

Acknowledgements

We are grateful to H. Cremades and A.M. Gulisano for useful discussions. NSS, GDC, and CHM acknowledge financial support from grant PICT 2007-1790 (ANPCyT). GDC and CHM acknowledge grants UBACyT 20020100100733 and PIP 2009-100766 (CONICET). ADL thanks CNPq for supporting this work under projects 303798/2008-4 and 481368/2010-8.

References

Attrill, G., Nakwacki, M.S., Harra, L.K., van Driel-Gesztelyi, L., Mandrini, C.H., Dasso, S., Wang, J. Using the evolution of coronal dimming regions to probe the global magnetic field topology. Sol. Phys. 238, 117–139, 2006.

Bisi, M.M., Breen, A.R., Jackson, B.V., Fallows, R.A., Walsh, A.P., Mikić, Z., Riley, P., Owen, C.J., Gonzalez-Esparza, A., Aguilar-Rodriguez, E., Morgan, H., Jensen, E.A., Wood, A.G., Owens, M.J., Tokumaru, M., Manoharan, P.K., Chashei, I.V., Giunta, A.S., Linker, J.A., Shishov, V.I., Tyul'Bashev, S.A., Agalya, G., Glubokova, S.K., Hamilton, M.S., Fujiki, K., Hick, P.P., Clover, J.M., Pintér, B. From the Sun to the Earth: the 13 May 2005 coronal mass ejection. Sol. Phys. 265, 49–127, 2010.

Borrini, G., Gosling, J.T., Bame, S.J., Feldman, W.C. Helium abundance enhancements in the solar wind. Jour. of Geophys. Res. 87, 7370–7378, 1982.

Brueckner, G.E., Delaboudiniere, J.-P., Howard, R.A., Paswaters, S.E., St. Cyr, O.C., Schwenn, R., Lamy, P., Simnett, G.M., Thompson, B., Wang, D. Geomagnetic storms caused by coronal mass ejections (CMEs): March 1996 through June 1997. Geophys. Res. Lett. 25, 3019–3022, 1998.

Brueckner, G.E., Howard, R.A., Koomen, M.J., Korendyke, C.M., Michels, D.J., Moses, J.D., Socker, D.G., Dere, K.P., Lamy, P.L., Llebaria, A., Bout, M.V., Schwenn, R., Simnett, G.M., Bedford, D.K., Eyles, C.J. The large angle spectroscopic coronagraph (LASCO). Sol. Phys. 162, 357–402, 1995.

Burlaga, L., Sittler, E., Mariani, F., Schwenn, R. Magnetic loop behind an interplanetary shock-Voyager, Helios, and IMP 8 observations. J. Geophys. Res. 86, 6673–6684, 1981.

Cane, H.V., Richardson, I.G., Cyr, O.C.S. Coronal mass ejections, interplanetary ejecta and geomagnetic storms. Geophys. Res. Lett. 27, 3591–3594, 2000.

Chandra, R., Pariat, E., Schmieder, B., Mandrini, C.H., Uddin, W. How can a negative magnetic helicity active region generate a positive helicity magnetic cloud? Sol. Phys. 261, 127–148, 2010.

Chapman, S., Bartels, J., 1940. Geomagnetism: Geomagnetic and Related Phenomena, vol. 1. Oxford, Clarendon Press, 1940, p. 542

Cid, C., Saiz, E., Cerrato, Y. Comment on "Interplanetary conditions leading to superintense geomagnetic storms (Dst $\leqslant -250$ nT) during solar cycle 23" by E. Echer et al.. Geophys. Res. Lett. 35, 21107, 2008.

Dal Lago, A., Gonzalez, W.D., Balmaceda, L.A., Vieira, L.E.A., Echer, E., Guarnieri, F.L., Santos, J., da Silva, M.R., de Lucas, A., Clua de Gonzalez, A.L., Schwenn, R., Schuch, N.J. The 17–22 October (1999) solar-interplanetary-geomagnetic event: very intense geomagnetic storm associated with a pressure balance between interplanetary coronal mass ejection and a high-speed stream. J. Geophys. Res. (Space Physics) 111, A07S14, 2006.

Dal Lago, A., Schwenn, R., Gonzalez, W.D. Relation between the radial speed and the expansion speed of coronal mass ejections. Adv. Spac. Res. 32, 2637–2640, 2003.

Dal Lago, A., Vieira, L.E.A., Echer, E., Gonzalez, W.D., Clúa de Gonzalez, A.L., Guarnieri, F.L., Balmaceda, L., Santos, J., da Silva, M.R., de Lucas, A., Schuch, N.J. Great geomagnetic storms in the rise and maximum of solar cycle 23. Braz. Jour. Phys. 34, 1542–1546, 2004a.

Dal Lago, A., Vieira, L.E.A., Echer, E., Gonzalez, W.D., de Gonzalez, A.L.C., Guarnieri, F.L., Schuch, N.J., Schwenn, R. Comparison between Halo CME expansion speeds observed on the Sun, the related shock transit speeds to Earth and corresponding ejecta speeds at 1 AU. Sol. Phys. 222, 323–328, 2004b.

Dasso, S., Mandrini, C.H., Démoulin, P., Luoni, M.L. A new model-independent method to compute magnetic helicity in magnetic clouds. Astron. Astrophys. 455, 349–359, 2006.

Dasso, S., Mandrini, C.H., Schmieder, B., Cremades, H., Cid, C., Cerrato, Y., Saiz, E., Démoulin, P., Zhukov, A.N., Rodriguez, L., Aran, A., Menvielle, M., Poedts, S. Linking two consecutive nonmerging magnetic clouds with their solar sources. J. Geophys. Res. (Space Physics) 114, A02109, 2009.

Delaboudiniere, J.-P., Artzner, G.E., Brunaud, J., Gabriel, A.H., Hochedez, J.F., Millier, F., Song, X.Y., Au, B., Dere, K.P., Howard, R.A., Kreplin, R., Michels, D.J., Moses, J.D., Defise, J.M., Jamar, C., Rochus, P., Chauvineau, J.P., Marioge, J.P., Catura, R.C., Lemen, J.R., Shing, L., Stern, R.A., Gurman, J.B., Neupert, W.M., Maucherat, A., Clette, F., Cugnon, P., van Dessel, E.L. EIT: extreme-ultraviolet imaging telescope for the SOHO mission. Sol. Phys. 162, 291–312, 1995.

Démoulin, P. A review of the quantitative links between CMEs and magnetic clouds. Ann. Geophys. 26, 3113–3125, 2008.

Démoulin, P., Mandrini, C.H., van Driel-Gesztelyi, L., Thompson, B.J., Plunkett, S., Kovári, Z., Aulanier, G., Young, A. What is the source of the magnetic helicity shed by CMEs? The long-term helicity budget of AR 7978. Astron. Astrophys. 382, 650–665, 2002.

Echer, E., Gonzalez, W.D., Tsurutani, B.T. Interplanetary conditions leading to superintense geomagnetic storms (Dst $\leqslant -250$ nT) during solar cycle 23. Geophys. Res. Lett. 35, 6, 2008a.

Echer, E., Gonzalez, W.D., Tsurutani, B.T., Gonzalez, A.L.C. Interplanetary conditions causing intense geomagnetic storms (Dst $\leqslant -100$ nT) during solar cycle 23 (1996-2006). J. Geophys. Res. (Space Physics) 113 (A12), A05221, 2008b.

Fan, Y. Magnetic fields in the solar convection zone. Living Rev. Sol. Phys. 6, 4, +, 2009.

Fan, Y., Zweibel, E.G., Linton, M.G., Fisher, G.H. The rise of kink-unstable magnetic flux tubes and the origin of delta-configuration sunspots. Astrophys. J. 521, 460–477, 1999.

Feminella, F., Storini, M. Large-scale dynamical phenomena during solar activity cycles. Astron. Astrophys. 322, 311–319, 1997.

Fok, M.C., Moore, T.E., Kozyra, J.U., Ho, G.C., Hamilton, D.C. Three-dimensional ring current decay model. J. Geophys. Res. 100, 9619–9632, 1995.

Gonzalez, W.D., Echer, E., Clúa de Gonzalez, A.L., Tsurutani, B.T., Lakhina, G.S. Extreme geomagnetic storms, recent Gleissberg cycles and space era-superintense storms. J. Atmos. Solar-Terres. Phys. 73, 1447–1453, 2011a.

Gonzalez, W.D., Echer, E., Tsurutani, B.T., Clúa de Gonzalez, A.L., Dal Lago, A. Interplanetary origin of intense, superintense and extreme geomagnetic storms. Space Sci. Rev. 158, 69–89, 2011b.

Gonzalez, W.D., Joselyn, J.A., Kamide, Y., Kroehl, H.W., Rostoker, G., Tsurutani, B.T., Vasyliunas, V.M. What is a geomagnetic storm? J. Geophys. Res. 99, 5771–5792, 1994.

Gonzalez, W.D., Tsurutani, B.T. Criteria of interplanetary parameters causing intense magnetic storms (Dst of less than-100 nT). Planet. Space Sci. 35, 1101–1109, 1987.

Gonzalez, W.D., Tsurutani, B.T., Lepping, R.P., Schwenn, R. Interplanetary phenomena associated with very intense geomagnetic storms. J. Atmos. Solar-Terres. Phys. 64, 173–181, 2002.

Gopalswamy, N., Yashiro, S., Liu, Y., Michalek, G., Vourlidas, A., Kaiser, M.L., Howard, R.A. Coronal mass ejections and other extreme characteristics of the 2003 October-November solar eruptions. J. Geophys. Res. (Space Physics) 110, A09S15, 2005.

Gopalswamy, N., Yashiro, S., Michalek, G., Stenborg, G., Vourlidas, A., Freeland, S., Howard, R. The SOHO/LASCO CME Catalog. Earth Moon Planet. 104, 295–313, 2009.

Gosling, J.T., Baker, D.N., Bame, S.J., Feldman, W.C., Zwickl, R.D., Smith, E.J. Bidirectional solar wind electron heat flux events. J. Geophys. Res. 92, 8519–8535, 1987.

Gosling, J.T., Pizzo, V., Bame, S.J. Anomalously low proton temperatures in the solar wind following interplanetary shock waves- evidence for magnetic bottles? J. Geophys. Res. 78, 2001–2009, 1973.

Harra, L.K., Crooker, N.U., Mandrini, C.H., van Driel-Gesztelyi, L., Dasso, S., Wang, J., Elliott, H., Attrill, G., Jackson, B.V., Bisi, M.M. How does large flaring activity from the same active region produce oppositely directed magnetic clouds? Sol. Phys. 244, 95–114, 2007.

Hudson, H.S., Labonte, B.J., Sterling, A.C., Watanabe, T., NOAA 7978: The last best old-cycle region? In: Watanabe T. Kosugi T. & Sterling A.C. (Ed.), Observational Plasma Astrophysics: Five Years of Yohokh and Beyond. 1998 pp. 237–244.

Klein, L.W., Burlaga, L.F. Interplanetary magnetic clouds at 1 AU. J. Geophys. Res. 87, 613–624, 1982.

Linton, M.G., Dahlburg, R.B., Fisher, G.H., Longcope, D.W. Nonlinear evolution of kink-unstable magnetic flux tubes and solar delta-spot active regions. Astrophys. J. 507, 404–416, 1998.

Liu, Y., Richardson, J.D., Belcher, J.W. A statistical study of the properties of interplanetary coronal mass ejections from 0 .3 to 5.4 AU. Planet. Space Sci. 53, 3–17, 2005.

Mandrini, C.H., Demoulin, P., Schmieder, B., Deluca, E.E., Pariat, E., Uddin, W. Companion event and precursor of the X17 flare on 28 October 2003. Sol. Phys. 238, 293–312, 2006.

Mandrini, C.H., Démoulin, P., van Driel-Gesztelyi, L., Green, L.M., López Fuentes, M.C. Magnetic helicity budget of solar-active regions from the photosphere to magnetic clouds. Astrophys. Space Sci. 290, 319–344, 2004.

Mandrini, C.H., Nakwacki, M.S., Attrill, G., van Driel-Gesztelyi, L., Démoulin, P., Dasso, S., Elliott, H. Are CME-related dimmings always a simple signature of interplanetary magnetic cloud footpoints? Sol. Phys. 244, 25–43, 2007.

McComas, D.J., Bame, S.J., Barker, P., Feldman, W.C., Phillips, J.L., Riley, P., Griffee, J.W. Solar wind electron proton alpha monitor (SWEPAM) for the advanced composition explorer. Space Sci. Rev. 86, 563–612, 1998.

Ontiveros, V., Gonzalez-Esparza, J.A. Geomagnetic storms caused by shocks and ICMEs. J. Geophys. Res. (Space Physics) 115 (A14), A10244, 2010.

Poisson, M., López Fuentes, M., Mandrini, C.H., Démoulin, P., Pariat, E., Study of magnetic flux emergence and related activity in active region NOAA 10314, 51, 1834–1841, 2013.

Rodriguez, L., Zhukov, A.N., Cid, C., Cerrato, Y., Saiz, E., Cremades, H., Dasso, S., Menvielle, M., Aran, A., Mandrini, C., Poedts, S., Schmieder, B. Three frontside full halo coronal mass ejections with a nontypical geomagnetic response. Space Weather 70, S06003, 2009.

Rostoker, G., Fälthammar, C.-G. Relationship between changes in the interplanetary magnetic field and variations in the magnetic field at the Earth's surface. J. Geophys. Res. 72, 5853, +, 1967.

Scherrer, P.H., Bogart, R.S., Bush, R.I., Hoeksema, J.T., Kosovichev, A.G., Schou, J., Rosenberg, W., Springer, L., Tarbell, T.D., Title, A., Wolfson, C.J., Zayer, I. MDI engineering team. The solar oscillations investigation-Michelson Doppler imager. Sol. Phys. 162, 129–188, 1995.

Sheeley Jr., N.R., Howard, R.A., Koomen, M.J., Michels, D.J. Associations between coronal mass ejections and soft X-ray events. ApJ 272, 349–354, 1983.

Siscoe, G., MacNeice, P.J., Odstrcil, D. East-west asymmetry in coronal mass ejection geoeffectiveness. Space Weather 50, S04002, 2007.

Smith, C.W., L'Heureux, J., Ness, N.F., Acuña, M.H., Burlaga, L.F., Scheifele, J. The ACE magnetic fields experiment. Space Sci. Rev. 86, 613–632, 1998.

Tsuneta, S., Acton, L., Bruner, M., Lemen, J., Brown, W., Caravalho, R., Catura, R., Freeland, S., Jurcevich, B., Owens, J. The soft X-ray telescope for the SOLAR-A mission. Sol. Phys. 136, 37–67, 1991.

Tsurutani, B.T., Gonzalez, W.D., Kamide, Y., Arballo, J.K. Preface. AGU, 1997.

Tsurutani, B.T., Lee, Y.T., Gonzalez, W.D., Tang, F. Great magnetic storms. Geophys. Res. Lett. 19, 73–76, 1992.

van Driel-Gesztelyi, L., Evolution and Decay of Active Regions (Invited review). In: C.E. Alissandrakis & B. Schmieder (Eds.), Three-Dimensional Structure of Solar Active Regions, vol. 155 of Astron. Soc. of the Pacific CS. 1998, pp. 202–+.

von Humboldt, A. Die vollständigste aller bisherigen Beobachtungen über den Einfluss des Nordlichts auf die Magnetnadel angestellt. Annalen der Physik 29, 425–429, 1808.

Wang, C., Du, D., Richardson, J.D. Characteristics of the interplanetary coronal mass ejections in the heliosphere between 0.3 and 5.4 AU. J. Geophys. Res. (Space Physics) 110, A10107, 2005.

Wang, Y.M., Ye, P.Z., Wang, S. Multiple magnetic clouds: several examples during March-April 2001. J. Geophys. Res. (Space Physics) 108, 1370, 2003.

Wang, Y.M., Ye, P.Z., Wang, S., Zhou, G.P., Wang, J.X. A statistical study on the geoeffectiveness of Earth-directed coronal mass ejections from March 1997 to December 2000. J. Geophys. Res. (Space Physics) 107, 1340, 2002.

Webb, D.F., Hundhausen, A.J. Activity associated with the solar origin of coronal mass ejections. Sol. Phys. 108, 383–401, 1987.

Webb, D.F., Lepping, R.P., Burlaga, L.F., DeForest, C.E., Larson, D.E., Martin, S.F., Plunkett, S.P., Rust, D.M. The origin and development of the May 1997 magnetic cloud. J. Geophys. Res. 105, 27251–27260, 2000.

Xiong, M., Zheng, H., Wang, S. Magnetohydrodynamic simulation of the interaction between two interplanetary magnetic clouds and its consequent geoeffectiveness: 2 Oblique collision. J. Geophys. Res. (Space Physics) 114, A11101, 2009.

Xiong, M., Zheng, H., Wu, S.T., Wang, Y., Wang, S. Magnetohydrodynamic simulation of the interaction between two interplanetary magnetic clouds and its consequent geoeffectiveness. J. Geophys. Res. (Space Physics) 112, A11103, 2007.

Zhang, J., Dere, K.P., Howard, R.A., Bothmer, V. Identification of Solar Sources of Major Geomagnetic Storms between 1996 and 2000. Astrophys. J. 582, 520–533, 2003.

Zhang, J., Richardson, I.G., Webb, D.F., Gopalswamy, N., Huttunen, E., Kasper, J.C., Nitta, N.V., Poomvises, W., Thompson, B.J., Wu, C.-C., Yashiro, S., Zhukov, A.N. Solar and interplanetary sources of major geomagnetic storms ($Dst \leqslant -100$ nT) during 1996-2005. J. Geophys. Res. (Space Physics) 112, A10102, 2007.

Zhao, X., Feng, X., Wu, C.-C. Characteristics of solar flares associated with interplanetary shock or nonshock events at Earth. Jour. of Geophys. Res. (Space Physics) 111 (A10), A09103, 2006.

Zirin, H., Liggett, M.A. Delta spots and great flares. Sol. Phys. 113, 267–281, 1987.